Ultrasonic Imaging in Air with a Broadband Inverse Synthetic Aperture Sonar

Michael P. Hayes

Imaging and Sensing Team, Industrial Research Limited,
P.O. Box 20028, Christchurch, New Zealand
E-mail: m.hayes@irl.cri.nz

Abstract

An experimental ultrasound scanning sonar has been developed that uses a phased ultrasonic transducer array to image objects through the air. The sonar generates arbitrary long duration broadband signals and uses pulse compression to achieve a high range resolution and a high signal to noise ratio. This paper considers using the sonar in an inverse synthetic aperture side-scan configuration, where instead of moving a sonar past the objects of interest, they are moved past the fixed sonar, in this case using a conveyor system.

A high speed image reconstruction algorithm is presented for the production of diffraction limited imagery, based on recent developments in synthetic aperture radar/sonar spatial frequency domain (wavenumber) reconstruction algorithms, suitable for broadband (low Q) signals. Test results using the sonar are presented and its performance is discussed.

Finally, the paper concludes with a discussion of the practical difficulties with imaging in air using ultrasound and suggestions for using reference targets to ameliorate some of the medium induced phase abberations.

Keywords: *airborne ultrasound, aperture synthesis, image reconstruction, phase correction*

1. Introduction

An experimental scanning air sonar has been developed at the New Zealand Institute of Industrial Research that uses a phased ultrasonic transducer array to image objects through the air. The sonar generates arbitrary long duration broadband signals and uses pulse compression techniques to achieve a high range resolution and a high signal to noise ratio. The sonar has a large dynamic range to allow the detection of weakly scattered echoes in the presence of specular reflections.

The salient features of the scanning sonar system are [1, 2]:

- A multiple element broadband transmitter transducer (twenty elements 15 mm high by 2.2 mm wide on a 2.7 mm pitch) to generate a focused, steerable ultrasonic beam within the region of interest.
- Separate transmitter and receiver transducers to allow the transmission of long duration signals to ensure a high signal to noise ratio, and thus accuracy, at low peak power levels without the receiver being blind during transmission.
- Broadband operation (50–200 kHz) to give a high range resolution (2.3 mm) or a reduction in coherent speckle effects.
- Arbitrary waveform generation for each

transmitter transducer element to allow the formation of multiple, independent, transmitted beams. These beams can be focused at different positions to increase the scanning rate and can have different pulse compression codes to distinguish the echoes at the receiver.

- Digital demodulation of the echoes to ensure a large receiver dynamic range to cope with the small backscattered echoes from distant targets and the large specular echoes from close targets.
- Real-time digital pulse compression using a digital signal processor (TMS320C30).
- Interface to a host PC-AT computer running Linux with X windows for the user interface, image display, and image interpretation.

While this sonar system provides a very good range resolution, the lateral resolution of the sonar, orthogonal to the scanning direction, is much poorer. The lateral resolution is constrained by diffraction effects of a finite aperture and is proportional to the ratio of the ultrasonic wavelength to the transducer dimension. Thus to achieve a higher lateral resolution, shorter wavelengths or larger transducer dimensions are required.

While shorter wavelengths would be more desirable to improve the lateral resolution, they are more readily absorbed when propagating through air, and the transducer arrays would require considerable re-development, probably using micromachining techniques. Instead, this paper presents results from research performed to improve the lateral resolution of airborne ultrasound imaging systems by synthesising larger equivalent transducers.

2. Aperture synthesis

Aperture synthesis techniques have been developed in many different fields including microwave radar, underwater sonar, medical ultrasound, non-destructive testing, seismic imaging, and astronomical imaging [3]. Rather than physically constructing large transducer arrays, aperture synthesis relies on relative motion between the imaging system and the scene of interest. This motion allows the scene to be viewed over a greater field of view and thus by coherently combining the different views, a greater spatial bandwidth can be measured. From the reciprocity theorem of Fourier analysis, this greater spatial bandwidth allows a higher resolution image to be reconstructed.

This paper considers an inverse synthetic aperture side-scan configuration, where instead of moving a sonar past the objects of interest, they are moved past the fixed sonar, in this case using a stepper motor controlled table to simulate a conveyor system.

There have been a number of recent developments in high speed synthetic aperture reconstruction algorithms. The algorithm employed here, to reconstruct the scene reflectivity, is a modified version of the wavenumber algorithm [4, 5], suitable for broadband signals. Using continuous variables, suitably sampled for digital implementation, this algorithm is described as follows, where primed quantities denote a shifted origin:

Step 1: Pulse compress echoes and range gate the region of interest, of width $W_\tau = 2W_y/c$ centred on a delay $\tau_0 = 2y_0/c$, where c is the speed of sound propagation and y_0 is the distance from the sonar to the centre of the region:

$$\tilde{d}(x,\tau') = \text{rect}\left(\frac{\tau'}{W_\tau}\right)\int \tilde{e}(x,t+\tau'+\tau_0)\tilde{s}^*(t)dt.$$

Here $\tilde{s}^*(t)$ is the complex conjugate of the baseband transmitted signal (complex envelope) and $\tilde{e}(x,t)$ represents the received echoes at scene displacement x. (Note that this pulse compression operation is usually performed in the Fourier domain where the correlation simplifies to a multiplication. The sonar performs this operation in real-time on the DSP.)

Step 2: Perform a 2D Fourier transform, mapping the spatial displacement x and propagation delay τ' to spatial frequency u and temporal frequency f', respectively:

$$\begin{aligned}\tilde{D}(u,f') &= \mathcal{F}\left\{\tilde{d}(x,\tau')\right\},\\ &= \iint \tilde{d}(x,\tau')e^{-j2\pi(xu+f'\tau')}dxd\tau'.\end{aligned}$$

Step 3: Compensate for the amplitude frequency dependence and remove the phase

shifts commensurate with changing the delay origin to τ_0 and the spatial origin to $(0, y_0)$:

$$\tilde{G}(u,f') = \tilde{D}(u,f')\sqrt{1+f'/f_0}\times e^{j2\pi\tau_0\left[\sqrt{(f'+f_0)^2-(cu/2)^2}-(f'+f_0)\right]}.$$

Step 4: Perform the Stolt mapping operation:

$$H(u,v') = \mathcal{S}\left\{\tilde{G}(u,f')\right\},$$

where

$$v' = v - v_0 = \frac{2}{c}\left[\sqrt{(f'+f_0)-(cu/2)^2}-f_0\right],$$

describes the non-linear mapping of the temporal frequency f' and spatial frequency u to the spatial frequency v'. Note that this requires the sampled data to be re-interpolated.

Step 5: Inverse Fourier transform the spatial frequency data into the spatial domain:

$$\begin{aligned} h(x,y') &= \mathcal{F}^{-1}\left\{H(u,v')\right\}, \\ &= \iint H(u,v')e^{j2\pi(xu+y'v')}dudv'. \end{aligned}$$

Step 6: Remove the phase shift resulting from shifting the spatial frequency information in the v domain to baseband via the Stolt mapping operation:

$$\begin{aligned} \rho(x,y') &= h(x,y')e^{j2\pi v_0 y'}, \\ &= h(x,y')e^{j4\pi f_0 y'/c}. \end{aligned}$$

(Note that this step can be dispensed with if only the magnitude of the scene reflectivity is required.)

Step 7: Compensate for the range dependent amplitude variation to get an estimate of the scene reflectivity:

$$\hat{\sigma}(x,y') = \frac{\rho(x,y')}{\sqrt{y'+y_0}}.$$

A number of approximations are implicit in this algorithm, most importantly that the speed of relative sonar/target movement is small compared to the speed of propagation (so that Doppler effects are minimal) and that the Rayleigh-Gans (Born) approximation is applicable (i.e., the scattering is weak and multiple reflections are negligible [6]). With airborne ultrasound imaging, however, the latter is often violated and thus an iterative reconstruction approach may be required to reduce any artefacts resulting from multiple scattering.

3. Imaging results

The results presented here were obtained using the scanning air sonar mounted perpendicular to the travel of a stepper motor controlled table. The transmitter transducer array was oriented with its long axis vertical, so that it could be scanned in the vertical (z) direction), and with its short axis producing a poorer lateral resolution in the direction of the table movement (x). For these experimental measurements, the transmitter array was not scanned, but focused at a distance of 250 mm in the y-direction.

Linear frequency modulated chirp pulses were transmitted, with a nominal centre frequency of 150 kHz and bandwidth of 80 kHz, and the echoes from the targets were received by a receiver transducer, located beside the transmitter array. Each pulse had a duration of 0.5 ms and were repeated every 20 ms, during which time the stepper controlled table was moved 0.86 mm (giving an average speed of 43 mm/s). 128 pulses were transmitted giving a total table travel of 110 mm. (Note that the pulse repetition period was limited by the transfer rate between the DSP and host; the DSP can pulse compress the echoes every 3 ms.)

Steel rods with a diameter of 3 mm were used as idealised point targets, mounted vertically in the centre of the stepper table. The closest approach of these targets was approximately 250 mm from the sonar.

Figure 1(a) shows the magnitude of the raw compressed pulses from a single target to illustrate the point response of the system. After synthetic aperture processing, the lateral resolution can be seen to be markedly improved in Figure 1(b). Similarly, Figure 2(a) shows the raw image from two targets, with their centres separated by 15 mm in the x-direction. Note that the two targets are not resolvable in the raw image but are clearly separated in the processed image, Figure 2(b).

While the lateral resolution is markedly improved, the imagery is not diffraction limited as a result of a poor phase coherence due to sound speed variations. This is discussed in greater detail in the following section.

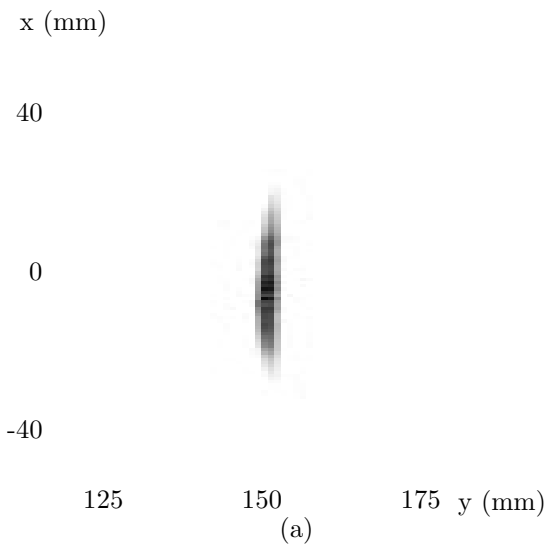

Figure 1: (a) magnitude of raw pulse compressed sub-image, $\left|\tilde{d}(x, c\tau'/2)\right|$ for a single point scatterer, and (b) magnitude of reconstructed sub-image, $|\hat{\sigma}(x, y')|$ for a single point scatterer, where $\Delta x = 0.86\,\text{mm}$ and $\Delta y = 1.15\,\text{mm}$.

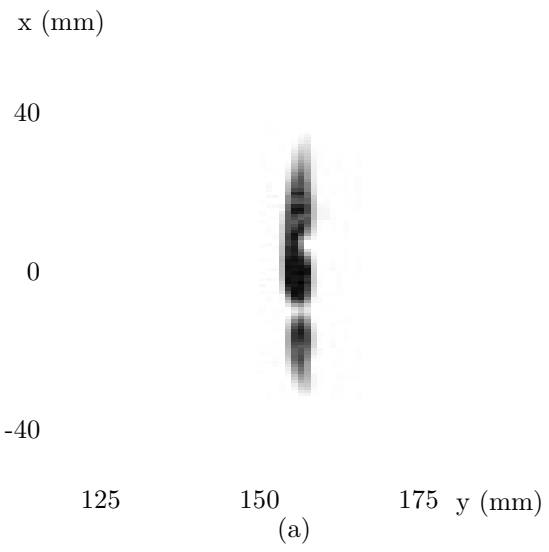

Figure 2: (a) magnitude of raw pulse compressed sub-image, $\left|\tilde{d}(x, c\tau'/2)\right|$, and for two point scatterers, and (b) magnitude of reconstructed sub-image, $|\hat{\sigma}(x, y')|$, for two point scatterers, where $\Delta x = 0.86\,\text{mm}$ and $\Delta y = 1.15\,\text{mm}$.

4. Phase correction

For an aperture to be successfully synthesised, phase coherence is required between the echoes measured across the length of the desired aperture. This phase coherence can be destroyed either by unknown relative motion between the sonar and targets or by medium fluctuations, usually as a result of convection currents. For high resolution imagery, it is essential that these fluctuations are smaller than an eighth of a wavelength [7].

To assess the phase stability of the air medium, a number of laboratory experiments were performed in a range of air conditions from still to extremely turbulent [8]. As

expected, the phase of the echo reflected from a stationary target was found to wander with time in the presence of draughts. Even with a slight, but perceptible, draught from an air-conditioning unit, the phase was observed to fluctuate by up to two radians over a fifteen second measurement interval for a stationary target at a 250 mm range (see Figure 3(a),(b)). This fluctuation is several orders of magnitude greater than the noise induced phase errors for a specular reflector and is large enough to destroy the phase coherence across the synthetic aperture. Even with comparatively still air, the phase was found to vary by up to 1 radian over the same interval. A second target, displaced 25 mm from the first target, was shown to have a phase variation highly correlated with that of the first target (see Figure 3(c)).

While the speed of sound in air varies with pressure, humidity, and temperature, the latter has the most affect. The approximate temperature dependence upon the speed of sound is $c \approx 20.05\sqrt{T}$, which yields a phase variation for a target at a range r of

$$\phi(T) \approx \frac{4\pi f_0 r}{20.05} T^{-\frac{1}{2}}, \tag{1}$$

Differentiating this with respect to the ambient temperature T, a temperature fluctuation of ΔT can be seen to produce a relative phase error of

$$\frac{\Delta\phi(t)}{\phi(T)} \approx \frac{-\Delta T}{2T}. \tag{2}$$

For example, a 1 K temperature fluctuation at $T = 293$ K produces a relative phase error of -0.17%. While this relative error may be small, the echo path length is usually many wavelengths long. For example, a target at a range $r = 225$ mm produces a phase shift of 1226 radians at $f_0 = 148.8$ kHz, corresponding to an absolute phase error of 2.1 radians—a significant phase error when considering that the phase can only be measured modulo 2π.

To maintain the accuracy of an air sonar ranging system in the presence of temperature fluctuations, it is desirable to utilise a known target within the field of view of the sonar. This known target can be used to recalibrate the propagation delay for each received echo from the target being measured [9]—this is preferable to indirectly determining the speed of sound propagation by monitoring the ambient temperature [10].

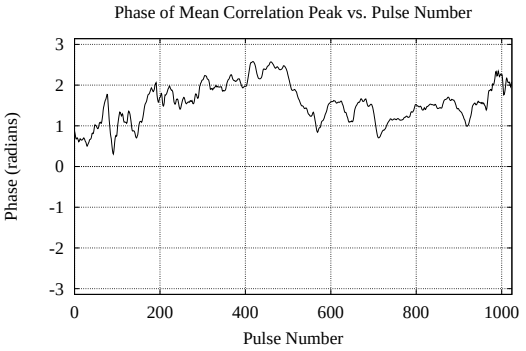

(a)

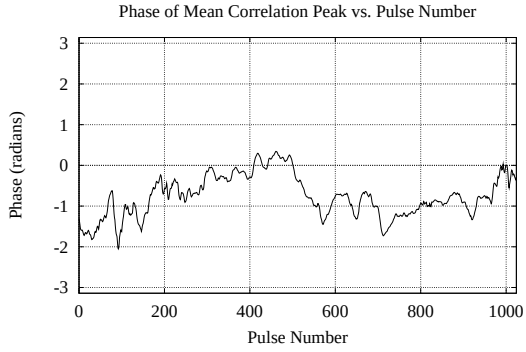

(b)

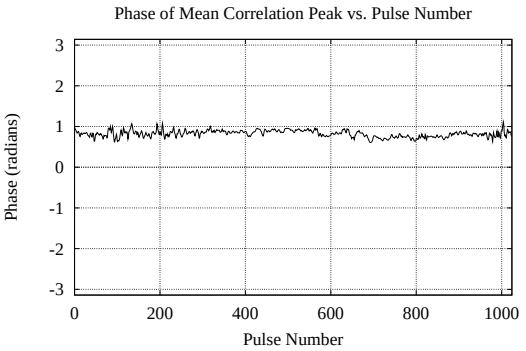

(c)

Figure 3: Magnitude and phase variation with time of echoes from two targets separated in range by 25 mm, (a) closest target phase ϕ_1 = 1.56, σ_{ϕ_1} = 0.48, (b) farthest target phase ϕ_2 = -0.76, σ_{ϕ_2} = 0.51, and (c) phase difference, $\phi_2 - \phi_1$ = 1.00, $\sigma_{\phi_2-\phi_1}$ = 0.05, at $T = 292.2$ K with noticeable draught. Measurements were obtained approximately every 15 ms. Note that the measured phases have been offset by $\pi/2$ to avoid wrap-arounds when plotting.

Preliminary experiments have shown that by employing a known reference target, the gross medium induced phase errors could be sufficiently compensated to ensure a coherent synthetic aperture, suitable for reconstruction of targets in the vicinity of the reference target. Further work will investigate extending this reference target concept by fixing multiple targets in the field of view of the sonar, separated in range so that they can be individually resolved.

5. Conclusion

While synthetic aperture imaging has the potential to greatly improve the lateral resolution of an ultrasonic air sonar imaging system, the performance is greatly dependent upon the phase stability of the medium. For high quality imagery, it is essential that the extent of aperture being synthesised is sampled over an interval faster than the coherence time of the medium.

The preliminary results presented in this paper show promise for the technique, but also indicate that corrections for the phase error are required to achieve diffraction limited imagery. It appears that one ore more reference targets in the field of view of the sonar are required to compensate for the gross speed of sound variations. This is an aspect of the author's current research. Further work will also investigate using redundancies in the echo data to estimate and correct the phase distortions [11, 12].

Acknowledgement

This work was funded by the New Zealand Foundation of Research, Science, and Technology under FRST contract CO8617.

References

[1] M. P. Hayes, "A multi-mode airborne ultrasound sonar," in *Proceedings of the New Zealand Image and Vision Computing Workshop*, pp. 101–106, Aug. 1995.

[2] M. P. Hayes, "Test results from a multi-mode air sonar," in *Proceedings of the New Zealand Image and Vision Computing Workshop*, pp. 207–212, Aug. 1996.

[3] M. P. Hayes and P. T. Gough, "Broadband synthetic aperture sonar," *IEEE Journal of Oceanic Engineering*, vol. 17, pp. 80–94, Jan. 1992.

[4] M. Soumekh, *Fourier Array Imaging*. Englewood Cliffs, New Jersey: Prentice-Hall, Inc., 1994.

[5] D. W. Hawkins, *Synthetic aperture imaging algorithms with application to wide bandwidth sonar*. PhD thesis, University of Canterbury, Oct. 1996.

[6] R. H. T. Bates, V. A. Smith, and R. D. Murch, "Manageable multidimensional inverse scattering theory," *Physics Reports*, vol. 201, pp. 187–277, Apr. 1991.

[7] B. D. Steinberg, *Principles of Aperture and Array System Design*. New York: John Wiley & Sons, Inc., 1976.

[8] M. P. Hayes, "Advanced non-contact ultrasonic imaging 1996–1997." Industrial Research Limited Report 742, June 1997.

[9] R. Hickling and S. P. Marin, "The use of ultrasonics for gauging and proximity sensing in air," *Journal of the Acoustics Society of America*, vol. 79, pp. 1151–1160, Apr. 1986.

[10] P. K. Chande and P. C. Sharma, "A fully compensated digital ultrasonic sensor for distance measurement," *IEEE Transactions on Instrumentation and Measurement*, vol. IM-33, pp. 128–129, June 1984.

[11] K. A. Johnson, M. P. Hayes, and P. T. Gough, "A method for estimating the sub-wavelength sway of a sonar towfish," *IEEE Journal of Oceanic Engineering*, vol. 20, Oct. 1995.

[12] T. Isernia, V. Pascazio, R. Pierri, and G. Schirinzi, "Synthetic aperture radar imaging from phase corrupted data," *IEE Proceedings on Radar, Sonar, and Navigation*, vol. 143, pp. 268–274, Aug. 1996.